Analyst

Accepted Manuscript

This article can be cited before page numbers have been issued, to do this please use: X. Li, L. Sun, X. Yang, K. Zhou, G. Zhang, Z. Tong, C. Wang and J. Sha, *Analyst*, 2019, DOI: 10.1039/C9AN00163H.

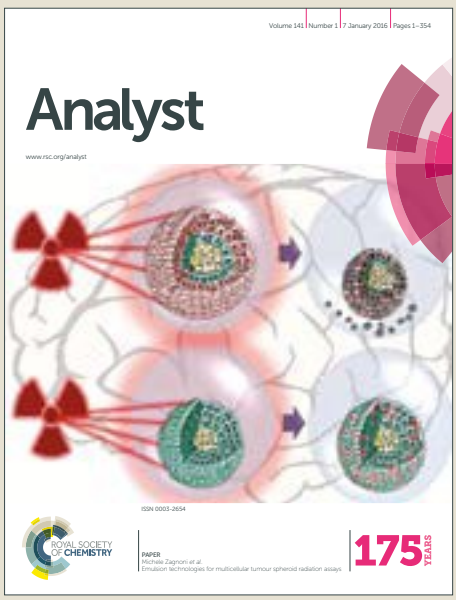

Journal Name

ROYAL SOCIETY OF CHEMISTRY View Article Online
DOI: 10.1039/C9AN00163H

ARTICLE

Enhancing colorimetric detection of H_2O_2 and ascorbic acid on polypyrrole coating fluconazole functionalized POMOFs

Received 00th January 20xx,
Accepted 00th January 20xx

DOI: 10.1039/x0xx00000x
www.rsc.org/

Xiao Li,[a] Longjiang Sun,[b] Xiya Yang,[a] Kunfeng Zhou,[a] Gongguo Zhang,[a] Zhibo Tong,[a] Cheng Wang,*[b,c] and Jingquan Sha*[a]

A new fluconazole functionalized polyoxometalate-based metal-organic frameworks (POMOFs), $[Ag_3(FKZ)_2(H_2O)_2][H_3SiW_{12}O_{40}]$ ($AgFKZSiW_{12}$) was successfully constructed, and its polypyrrole (PPy) coating composite $AgFKZSiW_{12}$@PPy was also obtained *via* a facile 'in situ' oxidation polymerization process. The peroxidase-like activity evaluation indicates that the maximized synergistic effect from the integration of PPy, SiW_{12} clusters, HFKZ drug molecules, and Ag ions deeply enhanced the overall performance. More importantly, $AgFKZSiW_{12}$@PPy exhibits the fastest respond time (30 s) among those of all reported peroxidase mimics to date, including the pristine $AgFKZSiW_{12}$ (2 min). Moreover, $AgFKZSiW_{12}$@PPy-based colorimetric biosensing platform towards H_2O_2 and ascorbic acid (AA) exhibits limit of detection (LOD) as low as 0.12 μM and 2.7 μM, respectively. This work reveals a promising prospect of colorimetric biosensors fabricating with high performance through the introduction of PPy in medical diagnosis and biotechnology.

Introduction

Hydrogen peroxide (H_2O_2), as a strong oxidant, has been widely used as disinfectant or bleaching agent in food, pharmaceutical, clinical and industrial aspects. However, overfull absorption of H_2O_2 in human body can result in poisoning for its strong erosion.[1-3] Meanwhile, ascorbic acid (AA), well known as a biological cofactor, is necessary for human health and plays an important role in many biochemical processes, and the deficiency or maladjustment of AA is linked to the symptoms of the cardiovascular disease and numerous types of cancers.[4-6] Therefore, for the sake of human health, the point-of-care detection of H_2O_2 and AA level in vitro motivates researchers to develop monitoring methods in fundamental research, even in live organism,[7] among which the most reported analytical techniques are the optical and electrochemical sensing approaches.[8-13] As we know that horseradish peroxidase (HRP) possesses great potential as a colorimetric diagnostic kit for H_2O_2, but it suffers from inherent disadvantages, such as the expensive cost and sophisticated preparation and purication.[14,15] So study on efficient HRP mimics is very eager, and a large number of smart materials have been found to exhibit intrinsic peroxidase-like activity similar to HRP, including iron based materials,[16] noble-metal materials,[17] metal oxides,[18,19] hybrid materials,[20] carbon-materials,[21,22] polymers,[23] and nanocomposites.[24-26] A fly in the ointment is that the above systems still sustain some shortcomings, such as the relatively long respond time and high detection limit.[27-29]

In the fields of catalysis, medicine, and material science, polyoxometalates (POMs) have exhibited promising properties owing to their tunable acid/base, redox, and catalytic properties.[30-32] Recently, $PW_{12}O_{40}$,[33] $SiW_{12}O_{40}$,[34] and tetra-nuclear zirconium-substituted POMs[35] have been authenticated excellent peroxidase-like activities toward H_2O_2 detection by catalytic oxidating of 3,3',5,5'-tetramethylbenzidine (TMB) to form a colored product.[36] However, the key challenge of relatively small surface areas (< 10 m^2 g^{-1}) and poor recovery issues hindered their further application.[37,38] To break this bottleneck, POMs have been incorporated into metal-organic frameworks (MOFs) to construct POM-based MOFs (POMOFs) with excellent stability and synergistic effect.[39-43] Among them, $Cu_6(Trz)_{10}(H_2O)_4[H_2SiW_{12}O_{40}]$ and $Na_4H_2[Cu_4(im)_{14}][Cu_3(H_2O)_3(BiW_9O_{33})_2]$ as peroxidase mimics have exhibited satisfactory peroxidase-like activities.[44,45] In contrast, the occurrence of drug molecules functionalized POMOFs as peroxidase mimics is particularly rare,[46] although many drugs have the potential to act as ligands , then the resulting POMOFs are particularly important both in POM chemistry and biochemistry. As a consequence, drug molecules functional POMOFs are highly desired in this field towards enhancing their application-related studies.

It is well known that modifying materials by the active substrates with high surface area maybe a feasible strategy to enhance catalytic performance. For instance, polyaniline (PANI)-modifying TiO_2 composite exhibited higher photocatalytic activity than that of TiO_2.[47] Besides, the peroxidase-like catalytic activity of the ternary hybrid FF@PW_{12}@GO with graphene oxide (GO) as

[a]*Department of Chemistry and Chemical Engineering, Jining University, Qufu 273155, P. R. China. *E-mail: shajq2002@126.com.*
[b]*School of Chemistry and Materials Science, Heilongjiang University, Harbin 150080, P. R. China. *E-mail: 1997059@hlju.edu.cn.*
[c]*Key Laboratory of Preparation and Application of Environmental Friendly Materials (Jilin Normal University), Ministry of Education, Changchun 130103, P. R. China.*
Electronic Supplementary Information (ESI) available: additional Figures and Tables. See DOI: 10.1039/x0xx00000x

View Article Online
DOI: 10.1039/C9AN00165H

supports enhanced 1.7 times than that of FF@PW_{12}.[48] Polypyrrole (PPy), as a conductive polymer, have been proved to possess large surface area and excellent absorption ability for dyes,[49] which is a suitable option for enhancing the catalytic performance of materials. Moreover, compared with PANI and polythiophene (PT), the polymerization process of PPy is mild and does not affect the stability of materials.[50-52] Up to now, significant progress has been made for the utilization of PPy as modification substrate through a facile process to advance performance.[53,54] Although PPy-based materials have great potential in optical/visual biosensing assays due to their deep black color, intense optical absorbance and good biocompatibility,[55] their peroxidase-like activity evaluation are still limited to PPy nanoparticle and PPy/Hemin nanocomposite.[56,57] This situation motivates us to expand the family of PPy-based colorimetric biosensors urgently.

Inspired by the aforementioned results, herein, a new drug molecule functionalized POMOFs, $[Ag_3(FKZ)_2(H_2O)_2][H_3SiW_{12}O_{40}]$ ($AgFKZSiW_{12}$) (HFKZ = 1-(2,4-difluorophenyl)-1,1-bis[(1H-1,2,4-triazol-1-yl)methyl] ethanol) was constructed by Keggin-type $H_4SiW_{12}O_{40}$, Ag ions and HFKZ molecules based on the following three aspects. Firstly, Keggin-type POMs are the most available, stable and successful POMs used in POMOFs construction to date. Secondly, Ag is the best electronic conductor and can adopt versatile coordination numbers (two to seven). In final, antifungal medicine HFKZ contains N-/O- mixed donors and exhibits flexible coordination modes. The peroxidase-like activity evaluation of $AgFKZSiW_{12}$ and $AgFKZSiW_{12}$@PPy were systematically performed and the results indicated that the coating of PPy on the surface of $AgFKZSiW_{12}$ effectively enhanced its peroxidase-like catalytic activity. In addition, the colorimetric biosensing towards H_2O_2 and AA detection with $AgFKZSiW_{12}$@PPy as peroxidase mimics was evaluated in detail for the first time (Scheme 1), which presents great application potentials in biotechnology and medical diagnosis.

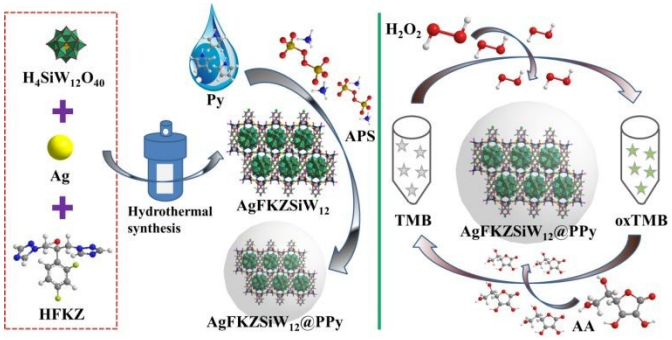

Scheme 1. Schematic illustration of the synthetic process of $AgFKZSiW_{12}$@PPy and as a bifunctional colorimetric biosensing platform.

Experimental Section

Materials and methods

All reagents with the analytical reagent grade were purchased commercially and were used without further purification. Deionized water was used throughout the whole experiment. The human serum samples used for AA determination were purchased from Nanjing SenBeiJia Biological Technology Co., Ltd. Elemental analyses (C, H, and N) were obtained on a PerkinElmer 2400 CHN Elemental Analyzer. The infrared (IR) spectra were performed on an Alpha Centaurt FT/IR spectrometer with KBr pellet in the region of 4000–400 cm^{-1}. Powder X-ray diffraction (PXRD) patterns were collected on a Rigaku Dmax 2000 X-ray diffractometer with graphite monochromatized Cu-Kα radiation (λ=0.154 nm) and 2θ ranging from 5 to 50°. The morphology and energy dispersive X-ray (EDX) analysis were operated on a scanning electron microscopy (SEM, Phenom ProX) with an accelerating voltage of 15 kV. X-ray photoelectron spectroscopy (XPS) measurements were carried out on a scanning X-ray microprobe (K-Alpha, Thermo Scientific) with Al kα radiation. The UV–vis diffuse reflectance spectra (DRS) were scanned on T9 spectrometer and the peroxidase-like catalytic activity evaluation was monitored in time scan mode at 661 nm using a Hitachi UV2010 spectrophotometer. Cyclic voltammetry (CV) experiments were obtained with a CHI 760E electrochemical workstation at room temperature.

Synthesis of $[Ag_3(FKZ)_2(H_2O)_2][H_3SiW_{12}O_{40}]$ ($AgFKZSiW_{12}$)

A mixture of $H_4SiW_{12}O_{40}$ (0.300 g, 0.10 mmol), $AgNO_3$ (0.200 g, 1.17 mmol), HFKZ (0.060 g, 0.20 mmol), NH_4VO_3 (0.036 g, 0.31 mmol) and H_2O (8 mL) was stirred for 30 min in air until it was homogeneous. When the pH value was adjusted to about 1.75 with 1 M HCl, the solution was transferred and sealed in a 23 mL Teflon-lined stainless steel autoclave, which was heated at 170 °C under autogenous pressure for 4 days. The yellow block crystals (Figure S1) were isolated and collected by filtration, washed thoroughly with distilled water, and dried at room temperature (45% yield based on W). Elemental analysis: $C_{26}H_{29}Ag_3F_4N_{12}O_{44}SiW_{12}$ (3847.33). Anal. Calcd: H, 0.75; C, 8.11; N, 4.36 (%). Found: H, 0.94; C, 8.08; N, 4.34 (%).

Synthesis of $AgFKZSiW_{12}$@PPy composite and PPy

Pyrrole (Py, 8.5 μL, 1.25×10^{-4} mol) was dissolved in 10 mL deionized water in a beaker. Then $AgFKZSiW_{12}$ (0.9617 g, 2.5×10^{-4} mol) was placed in the above solution and dispersed supersonically for 0.5 h. Finally, 5 mL ammonium persulfate (APS) solution (0.057 g, 2.5×10^{-4} mol) was slowly added to the above mixture as an oxidant. The product was stirred for 10 h, and then left undisturbed for 12 h. The resulting $AgFKZSiW_{12}$@PPy were separated, subsequently rinsed with water and alcohol, and finally dried at 60 °C in an oven for 24 h. PPy was obtained using a similar process to that used for the $AgFKZSiW_{12}$@PPy composite, except $AgFKZSiW_{12}$ was not added.

X-ray crystallographic study of $AgFKZSiW_{12}$

The crystal structure of $AgFKZSiW_{12}$ was determined from Single-crystal X-ray diffraction data. Intensity data were collected on a Bruker SMART CCD diffractometer equipped with a graphite monochromatized Mo-Kα radiation (λ = 0.71073 Å). The structure was solved by direct methods and difference Fourier map with SHELXL program,[58] and refined by full-matrix least-squares techniques on F^2. Anisotropic thermal parameters were used to refine all non-hydrogen atoms and the positions of hydrogen atoms on carbon atoms were calculated theoretically. Semiempirical absorption corrections were applied using the SADABS program. The crystal data and refinement parameters of $AgFKZSiW_{12}$ are summarized in Table S1. The selected bond lengths and bond angles of $AgFKZSiW_{12}$ are listed in Table S5.

View Article Online
DOI: 10.1039/C8AN00167H

Peroxidase-like activity evaluation

To evaluate the peroxidase-like activity of $AgFKZSiW_{12}$ and $AgFKZSiW_{12}$@PPy, the catalytic oxidation of TMB by H_2O_2 was tested. In a typical experiment, 0.6 mg/mL dispersion solution of materials was added into the acetate buffer solution (pH=3.5) containing 104 μM TMB and 83 μM H_2O_2 at 40 °C. The measurements were carried out by monitoring the absorbance change of TMB at 661 nm on a UV-vis spectrophotometer after the sample was transferred immediately to 1 cm quartz cuvette. To examine the influence of pH and temperature on the activity, the pH ranging from 3.0 to 7.0 and the reaction temperature from 25 to 60 °C were investigated, respectively.

Steady-state kinetics experiment

To get insight into the kinetic parameters of $AgFKZSiW_{12}$@PPy catalyzed reactions, the typical Michaelis–Menten model was used to evaluate the catalytic activity, and the apparent steady-state kinetic parameters were determined at the optimal condition by varying the concentrations of H_2O_2 (0.03 mM, 0.06 mM, 0.1 mM) and fixing the concentrations of TMB (0.04 mM), or varying the concentrations of TMB (0.04 mM, 0.08 mM, 0.12 mM) and fixing the concentrations of H_2O_2 (0.1 mM).

Michaelis-Menten curves were plotted according to Lineweaver-Burk plotting method by the following equation:

$$v=V_{max}\times[S]/(K_m+[S])$$

where v is the initial velocity, V_{max} represents the maximal reaction velocity, [S] corresponds to the concentration of substrate and K_m is the Michaelis constant.

H_2O_2 and AA colorimetric detection procedure

For H_2O_2 detection, various concentrations of H_2O_2 was added into the mixed solution and incubated at 40 °C for 5 min for standard curve measurement. The colorimetric detection assay of AA was also carried out as follows. $AgFKZSiW_{12}$@PPy (0.6 mg/mL) was added into the acetate buffer solution (pH=3.5) containing 104 μM TMB and 83 μM H_2O_2. Then AA with various concentrations was added to each of the mixture solutions, which were shaken and equilibrated for 60 s and then immediately filtered with a syringe filter. Finally, the mixed solution was monitored by UV–vis spectrometer directly at 661 nm. In order to measure the selectivity of $AgFKZSiW_{12}$@PPy in AA detection, several potential interfering solutions coexisting in real samples, including glucose and 4 kinds of cations (Na^+, K^+, Mg^{2+} and Ca^{2+}) were prepared (200 μM), respectively. For AA determination in serum samples, the samples were firstly treated by centrifugation at 12000 rpm for 30 min and then the supernatants were obtained for the next-step measurement.

Results and discussion

Structure and characterization of $AgFKZSiW_{12}$ and $AgFKZSiW_{12}$@PPy

Single-crystal X-ray diffraction analysis reveals that $AgFKZSiW_{12}$ crystallizes in monoclinic *C2/c* space group and the asymmetric unit consists of a half classical Keggin-type SiW_{12} polyanion, two Ag ions, one FKZ ligand and one water molecule (Figure S2a). Bond-valence sum (BVS) calculations[59] suggest that all W and Ag atoms are in the highest oxidation states, which is consistent with the crystal color, charge neutrality and coordination environments (Table S2). There are two crystallographically unique Ag ions with two distinct types of coordination geometries (Figure S2b), and the bond lengths and angles around Ag ions range from 2.134 to 2.364 Å for Ag-N and 175.85 to 180.0° for N-Ag-N, respectively.

$AgFKZSiW_{12}$ exhibits a glamorous three-dimensional POM-encapsulating metal-organic hybrid framework. More specifically, each FKZ links with three Ag ions (two Ag2 and one Ag1) giving birth to a two-dimensional Ag-FKZ layer containing hexa-nuclear $[Ag_6(FKZ)_6]$ cycles along the crystallographic *c*-axis (Figures 1a and 1b). What deserves to be mentioned here is that the two-dimensional Ag-FKZ layer exhibits the undulated feature along the crystallographic *abc* plane (Figure 1c). As a consequence, the vicinal identical two-dimensional Ag-FKZ layers are elaborately arranged in a parallel staggering mode fabricating a three-dimensional framework *via* C4–H4A···F2 bonds featuring spider-like subunits along *c*-axis and containing supramolecular Ag-FKZ nanocages with a window size of approximately 11.946×11.247 $Å^2$ as calculated with the closest distances along the crystallographic *abc* plane (Figures 1d and 1e). The size of Ag-FKZ cages is large enough to accommodate nanoscale Keggin POM polyanion. Finally, the SiW_{12} polyanions as "guest" clusters were encapsulated into the nanocages through the hydrogen bonds (C2–H2···O3, C5–H5···O1 and C12–H12···O15) as shown in Figures 1f, S3a and S3b. And this kind of packing arrangement may decrease the molecular repulsion with contrary charges and stabilize the whole crystal structure. Topological analysis using TOPOS40 software identifies that the overall three-dimensional supramolecular framework can be reduced to a unique (2,2,4,4)-connected topological network with the Schläfli symbol of $(4^4.6^2)(4^8.6^4.8^4)$ (Figure S3c). In this simplification, Ag1 and Ag2 both act as 2-connected nodes, while the SiW_{12} polyanions and FKZ ligands both act as 4-connected nodes.

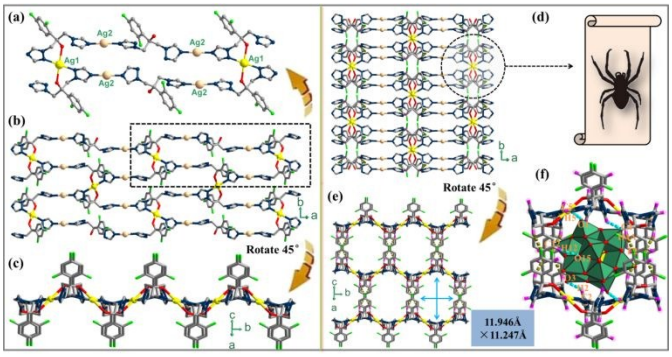

Fig. 1 Ball/stick representation of hexa-nuclear $[Ag_6(FKZ)_6]$ cycle (a), the two-dimensional layer along the *c*-axis (b) and along the *abc* plane (c), and the three-dimensional metal-organic framework with spider-like feature along the *c*-axis (d) and containing supramolecular nanocages along the *abc* plane (e), and detailed link mode between POMs and Ag-FKZ nanocages (f) in $AgFKZSiW_{12}$.

The diffraction peaks of both simulated and experimental PXRD patterns match well, revealing the phase purity of $AgFKZSiW_{12}$. The PXRD pattern of $AgFKZSiW_{12}$@PPy exhibits similar diffraction patterns to that of $AgFKZSiW_{12}$, illustrating that the structure of $AgFKZSiW_{12}$ is well retained during the polymerization of Py (Figure 2a). Furthermore, the peaks of PPy are not observed in

the pattern of $AgFKZSiW_{12}$@PPy, indicating that the amount of PPy may be too small to determine its existence. As shown in Figure 2b, IR spectrum of $AgFKZSiW_{12}$ exhibits four characteristic vibration peaks at 1077, 978, 898 and 817 cm^{-1} attributed to v_{as}(Si–O), v_{as}(W–O_d), v_{as}(W–O_b–W) and v_{as}(W–O_c–W), respectively. The band in the region of 1620-1140 cm^{-1} can be regarded as the stretching vibrations of FKZ molecules. In comparison, the according absorption bands from $AgFKZSiW_{12}$@PPy changed considerably, indicating slight variations in electron distribution of $AgFKZSiW_{12}$ due to strong electrostatic interaction between $AgFKZSiW_{12}$ and PPy. The successful introduction of PPy was also confirmed by the appearance of the characteristic peaks at about 1040, 1397 and 1547 cm^{-1} ascribed to the stretching vibrations of Py ring groups at the according positions in $AgFKZSiW_{12}$@PPy. Moreover, the morphologies of $AgFKZSiW_{12}$, PPy and $AgFKZSiW_{12}$@PPy (Figures 2c-2e) were investigated with SEM images. It can be clearly observed that $AgFKZSiW_{12}$ exhibits a smooth surface and sharp fringe, and $AgFKZSiW_{12}$@PPy shows a coarse, irregular surface and circular fringe owing to the wrapping of PPy, which indicates that PPy has been successfully coated on the surface of $AgFKZSiW_{12}$. The EDX elemental mapping images indicates the presence and the homogenous distribution of C, O, Si, W, Ag, N, and F elements in $AgFKZSiW_{12}$ (Figure S4). Meanwhile, the EDX elemental mapping images and corresponding spectrometry of $AgFKZSiW_{12}$@PPy prove that every element (Ag, Si, W, N, C and F) distributes uniformly (Figures 2f and S5). X-ray photoelectron spectra (XPS) of $AgFKZSiW_{12}$@PPy have been used to evaluate its compositions. As shown in Figure S6a, the XPS spectrum of $AgFKZSiW_{12}$@PPy has demonstrated the coexistence of C, N, O, Ag, Si and W elements. The N 1s spectra confirm the generation of PPy (pyrrolic-N, about 400 eV) successfully, which could be divided into three peaks ascribed to –N= and –NH– segments (399.2 and 399.6 eV) in the backbone of PPy chains, while the peak at 400.6 eV belongs to the protonation states (–NH^+–) (Figure S6b). Three Gaussian peaks related with C-C/C=C, C-O and C-N/C=N (284.6, 285.4, and 286.3 eV respectively) have been presented in the XPS spectra of C 1s, respectively (Figure S6c). Two peaks at 37.48 eV and 35.35 eV may attribute to W^{6+} $4f_{5/2}$ and W^{6+} $4f_{7/2}$, respectively (Figure S6d). Furthermore, Ag 3d spectrum exhibits two main peaks of Ag^+ $3d_{3/2}$ at the binding of 373.2 eV and Ag^+ $3d_{5/2}$ at the binding of 367.2 eV, and they can clearly demonstrate the existence of Ag^+ (Figure S6e). The UV–vis diffuse reflectance spectra (DRS) of $AgFKZSiW_{12}$ and $AgFKZSiW_{12}$@PPy were employed to study their optical properties. As shown in Figure S7, $AgFKZSiW_{12}$@PPy displays strong absorption in the ultraviolet and visible light region, while the $AgFKZSiW_{12}$ was inactive under the visible light irradiation, which signifies that PPy is a suitable option for enhancing the photo response region of $AgFKZSiW_{12}$@PPy.

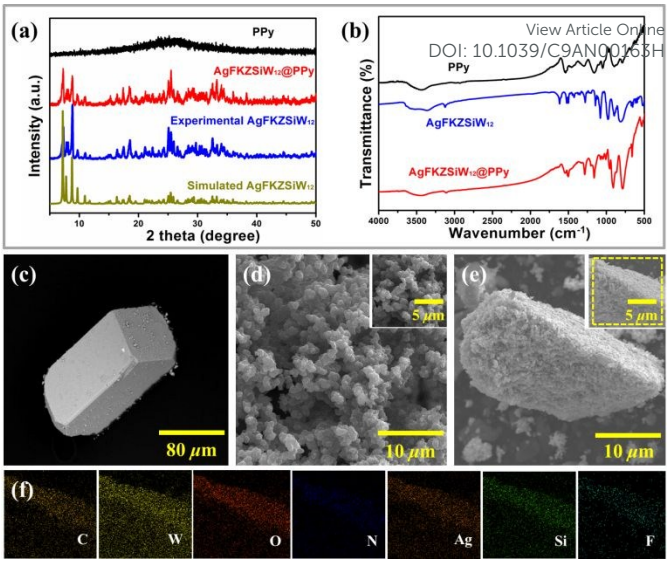

Fig. 2 PXRD patterns (a) and IR spectra (b) of $AgFKZSiW_{12}$, $AgFKZSiW_{12}$@PPy, and PPy. The SEM images of $AgFKZSiW_{12}$ (c), PPy (d), and $AgFKZSiW_{12}$@PPy (e) and EDX elemental mapping images of $AgFKZSiW_{12}$@PPy (f).

Peroxidase-like catalytic activity of $AgFKZSiW_{12}$@PPy

POMs and POMOFs as catalysts have been shown to demonstrate peroxidase-like activity for the detection of H_2O_2, so the peroxidase-like activities of $AgFKZSiW_{12}$ and $AgFKZSiW_{12}$@PPy were evaluated thoroughly by the catalytic oxidation of peroxidase substrate TMB by H_2O_2 and quantitatively monitored by recording UV–vis absorbance at 661 nm (Scheme S1). As shown in Figures 3a and S8a, with the addition of $AgFKZSiW_{12}$ or $AgFKZSiW_{12}$@PPy, a green color was gradually observed. UV–vis absorption tests show that the green solution exhibits remarkable absorption peaks at ca. 369, 452, and 661 nm, consistent with the reported results.[60,61] The absorbance intensity rose rapidly with the reaction time increasing. Note that $AgFKZSiW_{12}$@PPy exhibits rapid catalytically rate in only 30 s to observe color change by naked eyes, which is the best among those of all reported peroxidase mimics, including the $AgFKZSiW_{12}$ (2 min), to the best our knowledge. The fast discoloration time is attributed to the cooperation of stable $AgFKZSiW_{12}$ and PPy.

To identify the role of PPy coating on $AgFKZSiW_{12}$, some control experiments under similar conditions were performed (Figures 3b and S9). The solutions without TMB or H_2O_2 show negligible absorption in the range of 350-750 nm, indicating that both $AgFKZSiW_{12}$ and $AgFKZSiW_{12}$@PPy indeed possess peroxidase-like activity. Meanwhile, the solution without H_2O_2 shows negligible absorption identifying both $AgFKZSiW_{12}$ and $AgFKZSiW_{12}$@PPy lack oxidase-like activity, in which ROS of O* is generated from released O_2 and thus oxidate the oxidase substrate catalyzed by oxidase mimics. Although PPy itself also exhibits a certain degree of peroxidase-like catalytic activity (Figure S8b), the relative activity for $AgFKZSiW_{12}$@PPy was ~3 times higher than that of $AgFKZSiW_{12}$ and PPy, which is closely related to the combination of specific property of individual component and corresponding synergistic effect. More specifically, we know that higher affinity of catalyst with TMB and H_2O_2 is beneficial for enhancing the catalytic performance. When PPy were coated on the surface of $AgFKZSiW_{12}$, a smart microenvironment for the access of TMB and H_2O_2 maybe

View Article Online
DOI: 10.1039/C9AN00167H

generated, namely, hydrogen bonding between PPy and TMB could drive the movement of TMB and the loose stack of PPy around AgFKZSiW$_{12}$ may provide rational pathways for the movement of H_2O_2 toward AgFKZSiW$_{12}$@PPy. It is also worth mentioning that the introduction of PPy not only enhanced the heterogeneity of AgFKZSiW$_{12}$ but also improved the biocompatibility. Therefore, AgFKZSiW$_{12}$@PPy composite was used to perform the following peroxidase-like activity evaluation.

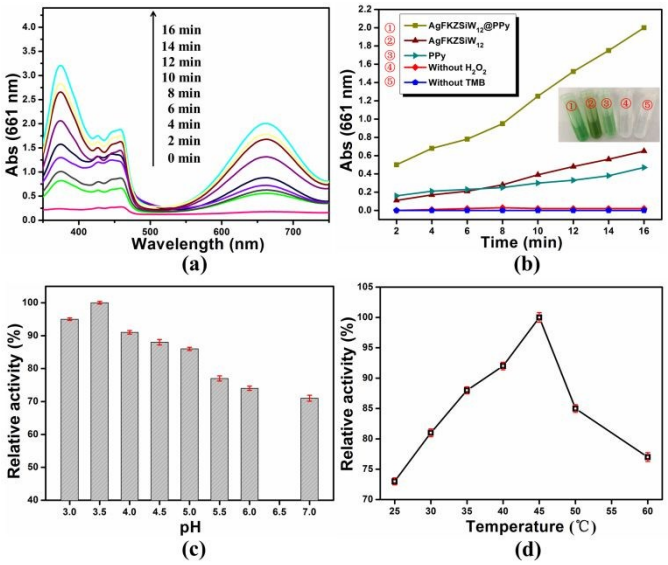

Fig. 3 (a) UV-vis absorption spectra of AgFKZSiW$_{12}$@PPy-catalyzed TMB colorimetric system as a function of reaction time from 0 to 16 min. (b) Time-dependent absorbance of control experiments at 661 nm: ①AgFKZSiW$_{12}$@PPy, H_2O_2, and TMB; ②AgFKZSiW$_{12}$, H_2O_2, and TMB; ③PPy, H_2O_2, and TMB; ④AgFKZSiW$_{12}$@PPy and TMB; ⑤AgFKZSiW$_{12}$@PPy and H_2O_2. Typical reaction conditions: acetate buffer solution (pH=3.5), H_2O_2 83 μM and TMB 104 μM at 40 °C. The inset shows the corresponding photographs. (c and d) Dependence of the peroxidase-like activity of AgFKZSiW$_{12}$@PPy on the reaction pH and reaction temperature (pH value: 3.0, 3.5, 4.0, 4.5, 5.0, 5.5, 6.0, 7.0; T: 25, 30, 35, 40, 45, 50, 60 °C).

Optimization of reaction conditions

Similar to HRP and other enzyme mimics,[62] the influence of pH, temperature and catalyst dosage on peroxidase-like catalytic activity of AgFKZSiW$_{12}$@PPy were explored shown in Figures 3c, 3d and S10. Above 70% relative activity could be maintained in the wide pH range of 3.0-7.0, which is a very meaningful signal to expand application of AgFKZSiW$_{12}$@PPy as enzyme mimics around physiological pH conditions. Apparently, the catalytic activity of AgFKZSiW$_{12}$@PPy is much higher in acidic media than neutral conditions, implying the oxidation of TMB proceeds more easily under acidic conditions, consistent with pristine HRP and many enzyme mimics.[63,64] The pH-dependent response curves shows the maximal intensity at pH 3.5 (Figure S10a), thus pH 3.5 was taken as the optimal pH value to achieve a higher peroxidase-like activity. Meanwhile, the influence of reaction temperature on the peroxidase-like activity was also tested (Figure S10b). With the increase of temperature, the absorbance at 661 nm increases gradually and reaches to the highest value at 45℃, indicating that the hyperthermal heating equipment is unnecessary in practical applications. Considering that AgFKZSiW$_{12}$@PPy possesses excellent catalytic activity at 40 ℃, which is closer to physiological temperature, 40 ℃ was adopted as the optimal reaction temperature to explore the peroxidase-like activity. In addition, when the AgFKZSiW$_{12}$@PPy dosage increased from 0.1 to 0.6 mg/mL (Figures S10c, S10d and S11), the absorbance increased slightly. After exceeding this point, the absorbance decreased gradually as dosage increasing. Therefore, the optimal AgFKZSiW$_{12}$@PPy dosage was 0.6 mg/mL.

Steady-state kinetic evaluation and cyclic voltammetry (CV) experiment of AgFKZSiW$_{12}$@PPy

It is known that K_m is an indicator of enzyme affinity to substrates and a smaller K_m value reflects a stronger affinity of enzyme for substrate and vice versa. As shown in Figures 4 and S12, and Table 1, the apparent K_m value for AgFKZSiW$_{12}$@PPy with H_2O_2 as substrate is smaller than that of AgFKZSiW$_{12}$, HRP and some other reported enzyme mimics, confirming AgFKZSiW$_{12}$@PPy has higher binding affinity for H_2O_2 than HRP and some other enzyme mimics. The result is consistent with the result of the maximal activity of AgFKZSiW$_{12}$@PPy. Meanwhile, the K_m value of AgFKZSiW$_{12}$@PPy with TMB as substrate is also lower than that of AgFKZSiW$_{12}$, HRP and some other reported materials, indicating that AgFKZSiW$_{12}$@PPy has a higher binding affinity for TMB than HRP and some other enzyme mimics. And the V_{max} value of AgFKZSiW$_{12}$@PPy with H_2O_2 as substrate is higher than HRP and some reported materials, demonstrating that AgFKZSiW$_{12}$@PPy possesses superior catalytic efficiency than HRP and other reported enzyme mimics. Previous reports have proved that PPy possesses large surface area and excellent absorption ability for dyes, which is beneficial to the capture of TMB and H_2O_2 molecules in solutions. So the above results indicate that AgFKZSiW$_{12}$@PPy possesses predominant peroxidase-like activity for the introduction of PPy enhanced the peroxidase-like activity of AgFKZSiW$_{12}$. As shown in Figure S13, we have also performed cyclic voltammetry (CV) experiments of AgFKZSiW$_{12}$ and AgFKZSiW$_{12}$@PPy. Obvious signals of electrocatalytic reduction of H_2O_2 on carbon paste electrodes (CPEs) modified by AgFKZSiW$_{12}$ and AgFKZSiW$_{12}$@PPy were both observed, which might be related to the electrocatalytic reduction ability of AgFKZSiW$_{12}$ and AgFKZSiW$_{12}$@PPy, and their high affinity with H_2O_2. Comparing with the signals of electrocatalytic reduction of H_2O_2 on AgFKZSiW$_{12}$-CPE, the signals on AgFKZSiW$_{12}$@PPy-CPE became larger. This might be related to the higher electrocatalytic reduction ability of AgFKZSiW$_{12}$@PPy, and also higher affinity between H_2O_2 and AgFKZSiW$_{12}$@PPy. The above results are consistent with our assumption that the introduction of PPy can facilitate the absorption of TMB or H_2O_2, which are two important factors for the catalytic performance enhancement.

View Article Online
DOI: 10.1039/C9AN00167H

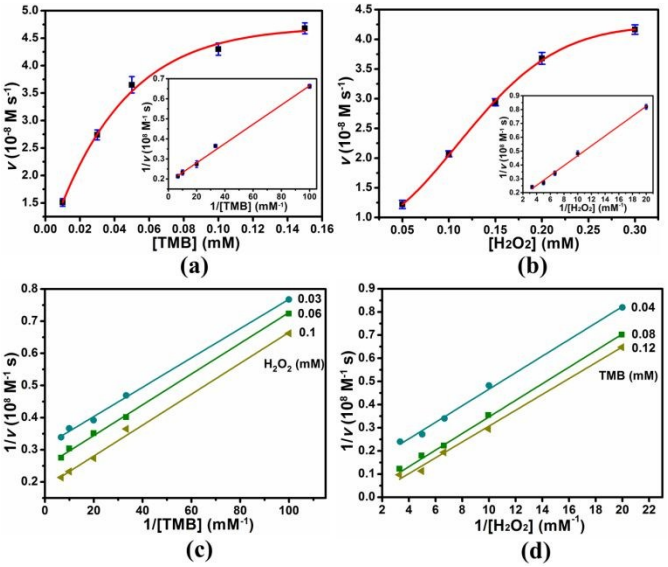

Fig. 4 Steady-state kinetic assays of AgFKZSiW$_{12}$@PPy: (a) 100 μM H_2O_2 with varying TMB concentration, (b) 40 μM TMB with varying H_2O_2 concentration. (c and d) Double reciprocal plots of the activity of AgFKZSiW$_{12}$@PPy with the concentration of H_2O_2 (0.03 mM; 0.06 mM; 0.1 mM) fixed and TMB fixed (0.04 mM; 0.08 mM; 0.12 mM). The reactions were performed in pH=3.5 buffer solution with AgFKZSiW$_{12}$@PPy (0.6 mg/mL) at 40 °C.

Table 1. K_m and V_{max} of AgFKZSiW$_{12}$, AgFKZSiW$_{12}$@PPy, and other reported enzyme mimics.

Enzyme mimics	H_2O_2		TMB		Ref.
	K_m (mM)	V_{max} (10^{-8} M s^{-1})	K_m (mM)	V_{max} (10^{-8} M s^{-1})	
HRP	3.7	8.71	0.434	10.00	[66]
Fe_3O_4 MNPs	154	9.78	0.098	3.44	[16]
PW_{12}	15.89	4.24×10^{-4}	0.11	43.1	[33]
FF@PW_{12}@GO	0.214	10.5	0.033	10.8	[47]
CuNPs@C	1.89	5.30	1.65	12.05	[67]
MOF-808	1.06	1.39	0.0796	3.12	[62]
BiW_9Cu_3	0.29	0.69	0.36	1.43	[45]
SbW_9Cu_3	0.25	0.71	0.14	0.64	[45]
AgFKZSiW$_{12}$	1.233	5.44	0.051	4.17	This work
AgFKZSiW$_{12}$@PPy	0.221	10.17	0.026	5.43	This work

Peroxidase-like catalytic mechanism of AgFKZSiW$_{12}$@PPy

As shown in Figures 4c and 4d, the double reciprocal plots of initial velocity *vs.* the concentration of one substrate were obtained over a range of concentrations of the second substrate. It is obvious that the slopes of all lines were almost parallel, indicating the possible ping-pong mechanism, which is similar to the observation for HRP and other reported enzyme mimics.[65] That is to say, AgFKZSiW$_{12}$@PPy binds and reacts with the first substrate, then releases the first product before reacting with the second substrate. Moreover, the nature of TMB catalytic reaction may originate from the generation of the hydroxyl radical (•OH) from the decomposition of H_2O_2 through electron transfer. As we know that terephthalic acid (TA) itself is non-fluorescent, but it can easily convert to highly fluorescent 2-hydroxyterephthalic acid (HTA) after reacting with •OH (Scheme S2). Therefore the highly sensitive and selective TA photoluminescence probing technique was used to confirm the formation of •OH. As shown in Figure S14, the fluorescence of TA was switched on upon the introduction of H_2O_2 and AgFKZSiW$_{12}$@PPy, and the fluorescence intensity of the solution containing AgFKZSiW$_{12}$@PPy was ~12 times higher than that in the absence of AgFKZSiW$_{12}$@PPy, indicating that AgFKZSiW$_{12}$@PPy could indeed activate H_2O_2 to generate •OH. Furthermore, the fluorescence intensity of the solution containing AgFKZSiW$_{12}$ is lower than that of AgFKZSiW$_{12}$@PPy, suggesting that less •OH is generated in the former case, consistent with the difference of peroxidase-like activities of these two systems.

Stability and reproducibility evaluation of AgFKZSiW$_{12}$@PPy

The reproducibility of peroxidase-like mimics is an important aspect for practical application. As shown in Figures S15, S16, and S17, the PXRD patterns and IR spectra of AgFKZSiW$_{12}$ and AgFKZSiW$_{12}$@PPy have exactly similarity of peak position before and after peroxidase-like activity evaluation, which confirms the ultrahigh stability of AgFKZSiW$_{12}$ and AgFKZSiW$_{12}$@PPy as peroxidase-like catalysts. Comparing with previous reported enzyme mimics based on Keggin-type POMs, the robustness of AgFKZSiW$_{12}$ and AgFKZSiW$_{12}$@PPy make them promising materials for a broad application in biodetection. Moreover, the recycled experiment of AgFKZSiW$_{12}$@PPy was performed (Figure S18), and the result shows that AgFKZSiW$_{12}$@PPy could be reused more than 4 times, which is superior than MOF-808 (reused 3 times).[62] The decrease of catalytic activity may be attributed to the aggregation of AgFKZSiW$_{12}$@PPy and the loss of AgFKZSiW$_{12}$@PPy during the centrifugation.

Detection of H_2O_2 and AA using AgFKZSiW$_{12}$@PPy

Given that the peroxidase-like activity of AgFKZSiW$_{12}$@PPy and the colour variation greatly dependent on the H_2O_2 concentration, the quantitative evaluation and colorimetric detection of H_2O_2 can be easily achieved on the basis of the relationship between the H_2O_2 concentration and the UV–vis absorbance intensity at 661 nm under the optimal conditions (40 ℃, pH 3.5). As shown in Figures 5a and 5b, the absorbance intensity increased as the H_2O_2 concentration increased in the range of 1 to 1000 μM, and the typical concentration-response curves of H_2O_2 show good linear correlation with the absorption intensity ranging from 1 to 100 μM. The linear regression equation could be expressed as $A=0.0154C_{H2O2}+0.0357$ ($R^2=0.998$). The limit of detection (LOD) was calculated as 0.12 μM (LOD=KS_0/S, where K is a numerical factor determined by the desirable confidence level, S_0 is the standard deviation (SD) of the blank measurements (n=10, K=3), and S is the slope of the calibration curve). The LOD is lower than that of the method using $Cu_6(Trz)_{10}(H_2O)_4[H_2SiW_{12}O_{40}]$ (1.37 μM), MOF-808 (4.5 μM) and other reported peroxidase mimics (Table S3), implying the superiority for the colorimetric sensing of H_2O_2. Simultaneously, the colour variation could be observed easily, which offers a facile and simple approach to detect H_2O_2 by the naked eyes even with low H_2O_2 concentration.

Remarkably, a trace amount of AA can considerably induce the two-electron reduction of oxTMB catalyzed by AgFKZSiW$_{12}$@PPy to

View Article Online
DOI: 10.1039/C9AN00163H

TMB and result in the color fading (Scheme S3). Based on these observations, a 'turn-off' colorimetric biosensor for detecting AA by $AgFKZSiW_{12}$@PPy could be readily developed. As shown in Figures 5c and 5d, the absorption intensity at 661 nm gradually decrease with AA concentrations increasing in the range of 1−1000 μM, and AA concentration-response curves show good linear correlation with the absorption intensity ranging from 1 to 80 μM, in which the linear regression equation could be expressed as $\Delta A=0.0196C_{AA}+0.0509$ ($R^2=0.996$). The LOD was estimated to be 2.7 μM, which is lower than some colorimetric sensors for AA detection, eg. MOF-808 (15 μM) and MIL-68 (6 μM) (Table S3).

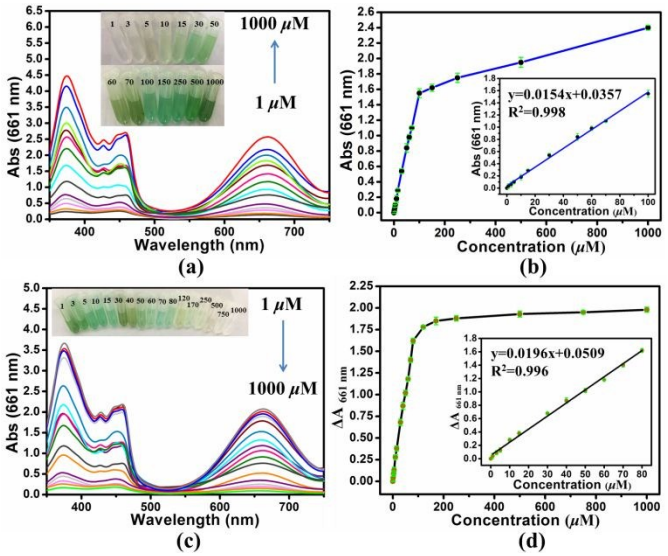

Fig. 5 (a) UV−vis spectra of TMB oxidation catalyzed by $AgFKZSiW_{12}$@PPy with various H_2O_2 concentrations and (b) concentration–response curve and corresponding linear calibration plot for H_2O_2 detection in buffer solution (pH=3.5) including $AgFKZSiW_{12}$@PPy (0.6 mg/mL). (c) UV−vis spectra of TMB oxidation catalyzed by $AgFKZSiW_{12}$@PPy with various AA concentrations as an inhibitor and (d) concentration–response curve and corresponding linear calibration plot for AA detection in buffer solution (pH=3.5) including $AgFKZSiW_{12}$@PPy (0.6 mg/mL). $\Delta A=A_0-A_i$ (A_0 and A_i are the absorbance at 661 nm before and after the addition of AA with a concentration of i, respectively).

Overall mechanism of H_2O_2 and AA colorimetric biosensing on $AgFKZSiW_{12}$@PPy

Based on the theoretical and experiment results, we elaborate the processes of H_2O_2 and AA colorimetric biosensing on $AgFKZSiW_{12}$@PPy and the possible mechanism is summarized in Figure 6. As proposed in the mechanism, SiW_{12} polyanions initially donate electrons and transfer them to the metal centers through trz ligands and PPy in the peroxidase-like catalytic reaction system. Then adsorbed H_2O_2 on $AgFKZSiW_{12}$@PPy was activated by metal centers to produce •OH coupling with the proton-electron transfer. Subsequently, desorbed •OH reacts with TMB molecules on the surface of $AgFKZSiW_{12}$@PPy to catalyse the oxidation of TMB and produce a green colour during the process of colorimetric biosensing. When AA was added into the above system as an inhibitor, oxTMB converts to TMB and AA converts to DHAA simultaneously, leading to the green colour fading.

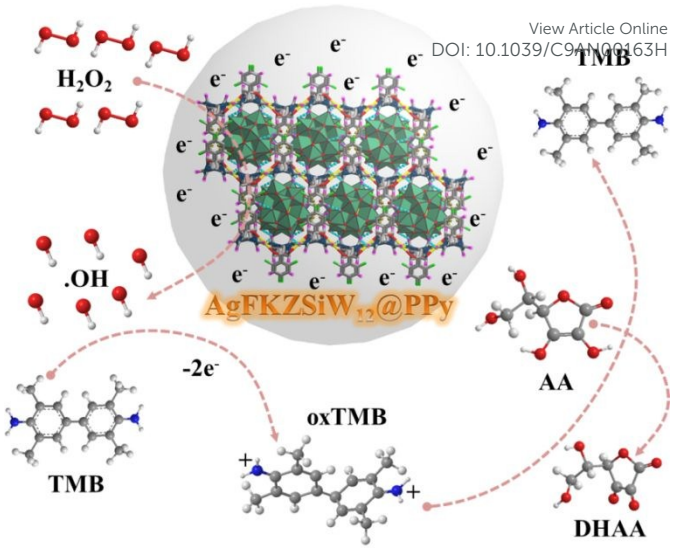

Fig. 6 Proposed mechanistic scheme for the H_2O_2 and AA colorimetric biosensing on $AgFKZSiW_{12}$@PPy.

Selectivity of AA detection and determination of AA in human serum samples

To evaluate the selectivity of this protocol for AA, possible coexisting substances in real samples including glucose and four kinds of cations (Na^+, K^+, Mg^{2+} and Ca^{2+}) were examined under the optimized conditions. The ΔA_{661nm} signals and corresponding photographic images of the $AgFKZSiW_{12}$@PPy–TMB–H_2O_2 system containing 50 μM AA and 4-fold other substances are shown in Figure 7a. Apparently, except for AA, other potential interferences have no evident effect on the ΔA_{661nm} signal and the color of the sensing system, demonstrating that the developed sensor has a superior selectivity for colorimetric detection of AA. To verify the performance of the sensing system for AA in practical applications, colorimetric detection in the presence of AA along with other possible interferences was also investigated (Figure 7b). The relative error of the interference effect of other biomolecules and common cations on detecting AA was less than 2.0%, which was considered to be tolerable. Therefore, it is concluded that the sensor responded specifically toward AA without interference of other substances, and the sensing platform is appropriate for the selective detection of AA in practical applications, which is comparable with Cu NPs@C.[67] Furthermore, the determination of AA in biological environment using our proposed colorimetric sensor has been performed. The concentration of AA in human serum sample is analysed and the results are displayed in Table S4. The recoveries of the sample are shown from 98.9% to 101.7%, demonstrating that the developed approach for AA determination in biological system is feasible and reliable.

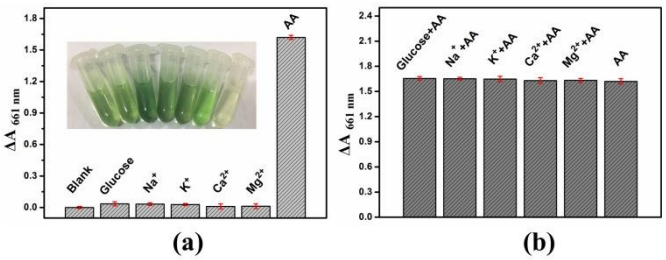

Fig. 7 Selectivity of $AgFKZSiW_{12}$@PPy for AA detection. (a) The $\Delta A_{661\ nm}$ signals of $AgFKZSiW_{12}$@PPy–TMB–H_2O_2 sensing system in the presence of

200 μM potential interferences; (b) The $\Delta A_{661\ nm}$ values of AgFKZSiW$_{12}$@PPy–TMB–H_2O_2 sensing system in the presence of 50 μM AA and 200 μM potential interferences. Various substances are glucose, Na^+, K^+, Ca^{2+}, Mg^{2+} and AA (from left to right). All reaction systems contain 0.6 mg/mL AgFKZSiW$_{12}$@PPy, 104 μM TMB and 83 μM H_2O_2, and the $A_{661\ nm}$ signals were collected at 120 s after initiation.

Conclusions

To sum up, the bifunctional AgFKZSiW$_{12}$@PPy composite with the excellent stability has been successfully prepared by coating the PPy on the surface of AgFKZSiW$_{12}$ *via* a facile 'in situ' method. Owing to the synergistic effect of PPy and AgFKZSiW$_{12}$, AgFKZSiW$_{12}$@PPy exhibits remarkably enhanced peroxidase-like catalytic activity, which is ca. 3 times higher than that of AgFKZSiW$_{12}$. Satisfactorily, based on the enhanced catalytic performance of AgFKZSiW$_{12}$@PPy and the biocompatibility of PPy, AgFKZSiW$_{12}$@PPy can be used as peroxidase mimics to detect H_2O_2 within the LOD of 0.12 μM in the range of 1−100 μM and AA within the LOD of 2.7 μM in the range of 1−80 μM. The visual detection of H_2O_2 and AA can be realized easily through the observable color change by bare eyes without any instrumentation. The work indeed opens up a facile and promising route for fabricating colorimetric biosensors with high performance through the introduction of PPy for medical diagnostics and biotechnology.

Conflicts of interest

There are no conflicts to declare.

Acknowledgements

Financial support from the Talent Culturing Plan for Leading Disciplines and the Natural Science Foundation (ZR2017LB001) of Shandong Province, and the Open Project Program of Key Laboratory of Preparation and Application of Environmental Friendly Materials (Jilin Normal University), Ministry of Education, China.

References

1 B. Wang, R. Q. Meng, L. H. Bi and L. X. Wu, *Dalton Trans.*, 2011, **40**, 5298-5301.
2 H. Jin, D. A. Heller, M. Kalbacova, J. H. Kim, J. Zhang, A. A Boghossian, N. Maheshri and M. S. Strano, *Nat. Nanotechnol.*, 2010, **5**, 302-309.
3 G. Jiang, H. Tang, L. Zhu, J. Zhang, and B. Lu, *Sens. Actuators B*, 2009, **138**, 607-612.
4 A. Tanaka, Y. Takeda, T. Nagasawa and K. Takahashi, *Solid State Commun.*, 2003, **126**, 191-196.
5 S. C. Rumsey and M. Levine, *J. Nutr. Biochem.*, 1998, **9**, 116-130.
6 O. Arrigoni, and M. C. De Tullio, *Biochim. Biophys. Acta Gen. Subj.*, 2002, **1569**, 1-9.
7 B. Yin, J. Deng, X. Peng, Q. Long, J. Zhao, Q. Lu, Q. Chen, H. Li, H. Tang, Y. Zhang and S. Yao, *Analyst*, 2013, **138**, 6551-6557.
8 S. S. Fan, M. G. Zhao, L. J. Ding, H. Li and S. G. Chen, *Biosens. Bioelectron.*, 2017, **89**, 846-852.
9 A. McNeillie, D. H. Brown, W. E. Smith, M. Gibson and L. Watson, *Dalton Trans.*, 1980, **5**, 767-770.
10 D. G. Duff, A. Baiker and P. P. Edwards, *Langmuir*, 1993, **9**, 2301-2309.
11 G. Liu and Y. Lin, *Electrochem. Commun.*, 2006, **8**, 251.
12 B. C. Dickinson and C. J. Chang, *J. Am. Chem. Soc.*, 2008, **130**, 9638-9639.
13 M. Zhou and S. Dong, *Acc. Chem. Res.*, 2011, **44**, 1232-1243.
14 C. Mateo, J. M. Palomo, G. Fernandez-Lorente, J. M. Guisan and R. Fernandez-Lafuente, *Enzyme Microb. Technol.*, 2007, **40**, 1451-1463.
15 N. C. Veitch, *Phytochemistry*, 2004, **65**, 249-259.
16 J. J. X. Wu, X. Y. Wang, Q. Wang, Z. P. Lou, S. R. Li, Y. Y. Zhu, L. Qin and H. Wei, *Chem. Soc. Rev.*, 2019, **48**, 1004-1076.
17 W. Song, B. Zhao, C. Wang, Y. Ozaki and X. F. Lu, *J. Mater. Chem. B*, 2019, **7**, 850-875.
18 R. Bhattacharjee, S. Tanaka, S. Moriam, M. K. Masud, J. Lin, S. M. Alshehri, T. Ahamad, R. R. Salunkhe, N. Nguyen, Y. Yamauchi, M. S. A. Hossain and J. A. S. Muhammad, *J. Mater. Chem. B*, 2018, **6**, 4783-4791.
19 S. Tanaka, M. K. Masud, Y. V. Kaneti, M. J. Shiddiky, A. Fatehmulla, A. M. Aldhafiri, W. A. Farooq, Y. Bando, M. S. A. Hossain and Y. Yamauchi, *ChemNanoMat*, 2019, **5**, 1-9.
20 L. Zhang, L. Han, P. Hu, L. Wang and S. Dong, *Chem. Commun.*, 2013, **49**, 10480-10482.
21 J. W. Zhang, H. T. Zhang, Z. Y. Du, X. Wang, S. H. Yu and H. L. Jiang, *Chem. Commun.*, 2014, **50**, 1092-1094.
22 H. J. Sun, Y. Zhou, J. S. Ren and X. G. Qu, *Angew. Chem. Int. Ed.*, 2018, **57**, 9224-9237.
23 M. Liu, H. Zhao, S. Chen, H. Yu and X. Quan, *Chem. Commun.*, 2012, **48**, 7055-7057.
24 K. Boriachek, M. K. Masud, C. Palma, H. P. Phan, Y. Yamauchi, M. S. A. Hossain, N. Nam-Trung, S. Salomon and M. J. Carlos, *Anal. Chem.*, 2019, **91**, 3827-3834.
25 M. K. Masud, S. Yadav, M. N. Islam, N. T. Nguyen, C. Salomon, R. Kline, H. R. Alamri, Z. A. Alothman, Y. Yamauchi, M. S. A. Hossain and M. J. Shiddiky, *Anal. Chem.*, 2017, **89**, 11005-11013.
26 G. Vinothkumar, A. I. Lalitha and K. S. Babu, *Inorg. Chem.*, 2018, **58**, 349-358.
27 A. Asati, S. Santra, C. Kaittanis, S. Nath and J. M. Perez, *Angew. Chem. Int. Ed.*, 2009, **121**, 2344-2348.
28 S. Liu, L. Wang, J. F. Zhai, Y. L. Luo and X. P. Sun, *Anal. Methods*, 2011, **3**, 1475-1477.
29 Y. Jv, B. X. Li and R. Cao, *Chem. Commun.*, 2010, **46**, 8017-8019.
30 Y. J. Chen, H. Y. Cao, W. B. Shi, H. Liu and Y. M. Huang, *Chem. Commun.*, 2013, **49**, 5013-5015.
31 C. L. Hill, *Chem. Rev.*, 1998, **98**, 1-2.
32 S. T. Zheng, J. Zhang, X. X. Li, W. H. Fang, G. Y. Yang, *J. Am. Chem. Soc.*, 2010, **132**, 15102-15103.
33 J. J. Wang, D. X. Han, X. H. Wang, B. Qi and M. S. Zhao, *Biosens. Bioelectron.*, 2012, **36**, 18-21.
34 S. Liu, J. Q. Tian, L. Wang, Y. W. Zhang, Y. L. Luo, H. Y. Li, A. M. Asiri, A. O. Al-Youbi and X. P. Sun, *ChemPlusChem*, 2012, **77**, 541-544.
35 D. Li, H. Han, Y. Wang, X. Wang, Y. Li, and E. Wang, *Eur. J. Inorg. Chem.*, 2013, **2013**, 1926-1934.
36 F. J. Ma, S. X. Liu, C. Y. Sun, D. D. Liang, G. J. Ren, F. Wei, Y. G. Chen and Z. M. Su, *J. Am. Chem. Soc.*, 2011, **133**, 4178-4181.
37 Z. Guo, X. Song, H. Lei, H. Wang, S. Su, H. Xu, G. Qian, H. Zhang and B. Chen, *Chem. Commun.*, 2015, **51**, 376-379.
38 X. Zhao, X. Bu, Q. G. Zhai, H. Tran and P. Feng, *J. Am. Chem. Soc.*, 2015, **137**, 1396-1399.
39 H. L. Li, M. Eddaoudi, M. O'Keeffe and O. M. Yaghi, *Nature*, 1999, **402**, 276-279.

View Article Online
DOI: 10.1039/C9AN00163H

40 C. Y. Sun, S. X. Liu, D. D. Liang, K. Z. Shao, Y. H. Ren and Z. M. Su, *J. Am. Chem. Soc.*, 2009, **131**, 1883-1888.
41 F. M. Zhang, L. Z. Dong, J. S. Qin, W. Guan, J. Liu, S. L. Li, M. Lu, Y. Q. Lan, Z. M. Su and H. C. Zhou, *J. Am. Chem. Soc.*, 2017, **139**, 6183-6189.
42 J. Q. Sha, X. Y. Yang, Y. Y. Chen, P. P. Zhu, Y. F. Song and J. Z. Jiang. *ACS Appl. Mater. Interfaces*, 2018, **10**, 16660-16665.
43 Y. Y. Wang, M. Zhang, S .L. Li, S. R. Zhang, W. Xie, J. S. Qin, Z. M. Su and Y. Q. Lan, *Chem. Commun.*, 2017, **53**, 5204-5207.
44 E. L. Zhou, C. Qin, P. Huang, X. L. Wang, W. C. Chen, K. Z. Shao and Z. M. Su, *Chem. Eur. J.*, 2015, **21**,11894-11898.
45 D. F. Chai, Z. Ma, H. Yan, Y. Qiu, H. Liu, H. D. Guo and G. G. Gao, *RSC Adv.*, 2015, **5**, 78771-78779.
46 X. Y. Li, D. S. Wang, G. X. Cheng, Q. Z. Luo, J. An and Y. H. Wang, *Applied Catalysis B: Environmental*, 2008, **81**, 267-273.
47 Z. Ma, Y. F. Qiu, H. H. Yang, Y. M. Huang, J. J. Liu, Y. Lu, C. Zhang and P. A. Hu, *ACS Appl. Mater. Interfaces*, 2015, **7**, 22036-22045.
48 X. X. Xu, X. Gao, Z. P. Cui, X. X. Liu and X. Zhang, *Dalton Trans.*, 2014, **43**, 13424-13433.
49 D. Chowdhury, A. Paul and A. Chattopadhyay, *Langmuir.*, 2005, **21**, 4123-4128.
50 Q. L. Li, C. R. Zhang and J. Q. Li, *J. Alloys Compd.*, 2011, **509**, 1953-1957.
51 D. Wang, Y. Wang, X. Li, Q. Luo, J. An and J. Yue, *Catal. Commun.*, 2008, **9**, 1162-1166.
52 B. Jin, F. Gao, Y. F. Zhu, X. Y. Lang, G. F. Han, W. Gao, Z. Wen, M. Zhao, J. C.Li and Q. Jiang, *Sci. Rep.*, 2016, **6**, 19317.
53 X. X. Xu, X. Gao, T. T. Lu, X. X. Liu and X. L. Wang, *J. Mater. Chem. A*, 2015, **3**, 198-206.
54 A. Ramanaviciene and A. Ramanavicius, *Crit. Rev. Anal. Chem.*, 2002, **32**, 245-252.
55 A. Ramanaviciene, A. Kausaite, S. Tautkus and A. Ramanavicius, *J. Pharm. Pharmacol.*, 2007, **59**, 311-315.
56 Y. Tao, E. G. Ju, J. S. Ren and X. G. Qu, *Chem. Commun.*, 2014, **50**, 3030-3032.
57 P. Hu, L. Han and S. J. Dong, *ACS Appl. Mater. Interfaces*, 2014, **6**, 500-506.
58 G. Sheldrick, SHELX-97, Program for Crystal Structure Refinement, University of Göttingen, *Germany* **1997**.
59 I. D. Brown and D. Altermatt, *Acta Crystallogr. Sect. B: Struct. Sci.*, 1985, **41**, 244-247.
60 S. Laing, A. Hernandez-Santana, J. Sassmannshausen, D. L. Asquith, I. B. McInnes, K. Faulds and D. Graham, *Anal. Chem.*, 2011, **83**, 297-302.
61 H. Q. Zheng, C. Y. Liu, X. Y. Zeng, J. Chen, J. Lü, R. G. Lin, R. Cao, Z. J. Lin and J. W. Su, *Inorg. Chem.*, 2018, **57**, 9096-9104.
62 H. Wang, K. W. Wan, and X. H. Shi, *Adv. Mater.*, 2018, 1805368.
63 X. Li, S. X. Li, Y. L. Wang, K. F. Zhou, P. P. Li and J. Q. Sha, *Polyhedron*, 2018, **151**, 206-212.
64 H. Wei and E. Wang, *Chem. Soc. Rev.*, 2013, **42**, 6060-6093.
65 N. Wang, B. C. Li, F. M. Qiao, J. C. Sun, H. Fan and S. Y. Ai, *J. Mater. Chem. B*, 2015, **3**, 7718-7723.
66 D. J. Porter and H. J. Bright, *J. Biol. Chem.*, 1983, **258**, 9913-9924.
67 H. L. Tan, C. J. Ma, L. Gao, Q. Li, Y. H. Song, F. G. Xu, T. Wang and L. Wang, *Chem. Eur. J.*, 2014, **20**, 16377-16383.

View Article Online
DOI: 10.1039/C9AN00163H

Table of contents

Enhancing colorimetric detection of H_2O_2 and ascorbic acid on polypyrrole coating fluconazole functionalized POMOFs

Xiao Li,[a] Longjiang Sun,[b] Kunfeng Zhou,[a] Gongguo Zhang,[a] Zhibo Tong,[a] Cheng Wang,*[b,c] and Jingquan Sha*[a]

[a]Department of Chemistry and Chemical Engineering, Jining University, Qufu 273155, P. R. China.

[b]School of Chemistry and Materials Science, Heilongjiang University, Harbin 150080, P. R. China.

[c]Key Laboratory of Preparation and Application of Environmental Friendly Materials (Jilin Normal University), Ministry of Education, Changchun 130103, P. R. China.

The bifunctional colorimetric biosensing platform based on polypyrrole coating fluconazole functionalized polyoxometalate-based metal-organic framework with ultrahigh stability for enhanced detection of H_2O_2 and ascorbic acid was developed for the first time.